Inverse agonist of ERRγ controls influenza A virus and SARS-CoV-2 infections by targeting SREBP-1c-mediated fatty acid biosynthesis

Kyoung-Oh Cho

choko@jnu.ac.kr

Chonnam National University https://orcid.org/0000-0002-5477-7021

Yeong-Bin Baek

Chonnam National University

Hyung-Jun Kwon

Korea Research Institute of Bioscience and Biotechnology

Hyung Jae Jeong

Bio-processing Technology Development and Support Team

Byungyoon Choi

Chonnam National University

Woo-Ram Park

Chonnam National University

Muhammad Sharif

Chonnam National University

Thu Nguyen

Chonnam National University https://orcid.org/0000-0002-5322-7298

Seong-Hun Jeong

Korea Research Institute of Bioscience and Biotechnology

In-Chul Lee

Korea Research Institute of Bioscience and Biotechnology https://orcid.org/0000-0001-8748-9731

Young-Bae Ryu

Functional Biomaterial Research Center

Mary Jasmin Ang

Chonnam National University

Jun-Gyu Park

Chonnam National University

Suk-Youl Park

Pohang University of Science and Technology

In-Sik Shin

Chonnam National University

Eunae Kim

Chosun University https://orcid.org/0000-0001-8538-7336

Changjong Moon

Chonnam National University https://orcid.org/0000-0003-2451-0374

Jeong-Sun Kim

Chonnam National University

Sunwoo Lee

Chonnam National University

Hyon choy

Chonnam Natl Univ Med School https://orcid.org/0000-0001-8853-1284

Seung-Soon Im

Keimyung University School of Medicine https://orcid.org/0000-0002-2743-2108

In-Kyu Lee

Kyungpook National University Hospital, School of Medicine https://orcid.org/0000-0002-1655-0985

Hoe-Yune Jung

Pohang University of Science and Technology

Dae-Eun Cheong

Chonnam National University

Dong Ju Lee

Chonnam National University https://orcid.org/0000-0002-0348-5694

Timothy Osborne

Johns Hopkins https://orcid.org/0000-0002-5150-4300

Tae-Il Jeon

Chonnam National University https://orcid.org/0000-0003-0655-8614

Don-Kyu Kim

Chonnam National University https://orcid.org/0000-0002-6251-6438

Hueng-Sik Choi

Chonnam National University

Article

Keywords:

Posted Date: August 19th, 2025

DOI: https://doi.org/10.21203/rs.3.rs-6651542/v1

Additional Declarations: Yes there is potential Competing Interest. K.-O.C. and D.J.L. are board members of Pharmacolinx, and H.-Y.J. and I.-K.L. are board members of NovMetaPharma. All other authors declare that they have no competing interests.

Abstract

The periodic emergence of pandemic RNA viral infections, such as COVID-19 and pandemic flus, and the declining efficacy of virus-targeting drugs underscore the need for innovative therapies. Here, we identify the nuclear receptor estrogen-related receptor gamma (ERRγ) as a key regulator of RNA virus replication through its role in reprogramming host fatty acid (FA) biosynthesis. Notably, heterozygous ERRγ knockout reduced influenza A virus (IAV) lung replication, thereby increasing the survival rate. Transactivation of ERRγ in the IAV- or SARS-CoV-2-infected cells was induced by the JNK/c-Jun signaling pathway. DN200434, an ERRγ-specific inverse agonist, showed broad-spectrum antiviral effects by inhibiting the sterol regulatory element-binding protein-1c (SREBP-1c)-dependent fatty acid biosynthesis, which is crucial for virus replication. The administration with DN200434 protected lethal IAV- or SARS-CoV-2-challenged animals. These findings identify ERRγ as a new proviral host factor, highlighting that targeting ERRγ to modulate SREPB-1c-dependent lipidomic reprogramming may represent a promising broad-spectrum antiviral strategy.

Main

The COVID-19 pandemic has highlighted the significance of emerging and reemerging zoonotic viral pathogens, such as highly pathogenic avian H5N1 influenza A virus (IAV), Ebola virus, and Zika virus[1–3]. Many of the recent notorious viral pathogens are RNA viruses with a high mutation rate due to their RNA-dependent RNA polymerase's lack of proofreading exonuclease activity[4]. This property eventually creates a wide variety of new variants with potential resistance to existing viral-protein-targeted antiviral drugs, such as IAV matrix-2 (M2) ion channel-targeting amantadine and IAV neuraminidase-targeting oseltamivir[4–6]. These have underscored a critical need to develop broad-spectrum host-directed antiviral drugs, which are less susceptible to viral resistance and effective in treating existing and newly emerging viral infections[5–7].

Nuclear receptors (NRs) are members of a large family of transcription factors that coordinate the regulation of a vast array of corresponding gene networks in response to hormonal, metabolic, developmental, and environmental signals[8,9]. Several viruses are known to exploit NRs to regulate the expression of their genes and/or optimize the cellular milieu to facilitate the viral life cycle[8]. Estrogen-related receptors (ERRs) are orphan NRs because their appropriate endogenous ligands have not yet been identified[9]. In mammals, there are three isoforms (ERRα, β, and γ, encoded by *Esrra*, *Esrrb*, and *Esrrg*, respectively), and the functions of ERRβ are restricted in mice, albeit not exclusively, to the maintenance of pluripotency in embryonic stem cells[10,11]. However, ERRα and ERRγ are broadly expressed in multiple organs and modulate many similar gene programs, such as energy metabolism and bone homeostasis[10,11]. ERRγ expression is highly inducible and dynamically regulated by membrane receptors that recognize diverse cell signals[9]. At present, it is unclear whether ERRs play a role in viral infections[12].

Since lipids and lipid droplets (LDs) play an important role in facilitating the life cycle of many diverse viruses at all levels, including viral entry, replication, and egress, lipid metabolism is an emerging potential target for antiviral intervention[13–16]. The liberated lipids, particularly free fatty acids (FFAs), serve as building blocks for the biogenesis of viral replication compartments, viral particle morphogenesis, or energy sources required for viral replication[13,15–18]. During the replication of diverse viruses, sterol regulatory element-binding proteins (SREBPs) transactivate genes involved in FA and cholesterol biosynthesis[16,19–21]. However, the regulation of SREBPs in cells infected by viruses is not well understood.

In this study, we demonstrate that ERRγ regulates host lipid metabolism to facilitate viral replication. Inhibition of ERRγ with inverse agonist DN200434 significantly blocks the replication of diverse RNA viruses by disrupting the viral protein palmitoylation, double-membrane vesicle (DMV) formation, and mitochondrial beta-oxidation. DN200434 also protected mice from lethal IAV infection and SARS-CoV-2-infected hamsters, while reducing lung lesions and eicosanoid and proinflammatory cytokine levels. These results suggest that the selective control of ERRγ transcriptional activity could be a potential therapeutic strategy for treating diverse RNA virus infections, such as SARS-CoV-2 and highly pathogenic avian influenza A virus (H5N1).

Results

ERRγ haploinsufficiency renders the mice resistant to IAV infection in vitro and in vivo

We first evaluated the sequential expression levels of ERRα and ERRγ during virus replication both *in vitro* and *in vivo*. In human lung epithelial A549 cells infected with IAV, ERRγ mRNA levels showed distinct dynamics with a gradual increase followed by a decline, accompanied by nuclear translocation (Fig. 1a,b). A similar biphasic expression pattern for ERRγ was observed in SARS-CoV-2-infected Vero E6 cells and lung tissues from animals challenged with IAV or SARS-CoV-2 (Extended Data Fig. 1). In contrast, ERRα mRNA levels remained unaffected during viral replication (Fig. 1a and Extended Data Fig. 1d-f). These results suggest a dynamic role for ERRγ as a host transcription factor during infection by different RNA viruses

To directly examine the role of ERRγ in viral replication, we first silenced ERRγ *in vitro* and infected cells with target viruses. ERRγ silencing significantly reduced the viral genome copy numbers for seven target viruses (Fig. 1c and Extended Data Fig. 2). To further investigate, we used ERRγ heterozygous mice (*Esrrg*$^{+/-}$) (Extended Data Fig. 3) to assess resistance to IAV infection, as homozygous ERRγ-null mice die shortly after birth[22]. The intranasal challenge of wild-type (WT) mice with 10^3 PFU of mouse-adapted IAV PR8 strain resulted in 100% mortality within 10 days, accompanied by severe body weight loss and clinical scores (Fig. 1d-f). In contrast, *Esrrg*$^{+/-}$ mice demonstrated significantly reduced mortality (50%), maintained body weight, and displayed milder clinical scores. ERRγ haploinsufficiency also diminished IAV protein synthesis, viral genome replication, and progeny viral production in the lungs compared to WT mice (Fig. 1g-i). Furthermore, histopathological analysis revealed that lung lesions caused by IAV

infection in WT mice were markedly ameliorated in *Esrrg*$^{+/-}$ mice, with fewer IAV antigen-positive cells observed (Fig. 1j). These data strongly suggest that ERRγ plays a critical role in facilitating RNA virus replication.

Upregulation of ERRγ through ROS-induced JNK/c-Jun signaling pathway

Oxidative stress induced by ROS is a common pathophysiological feature in viral infections[23,24]. As shown in Fig. 2a,b, IAV or SARS-CoV-2 infection significantly increased intracellular ROS levels, an effect that was reduced by treatment with the antioxidant N-acetylcysteine (NAC). Given that ERRγ is reported to function as a ROS sensor[25], we sought to determine whether virus-induced ROS transactivates ERRγ. Cells were transfected with a plasmid encoding the full-length *ERRγ* promoter-luciferase gene (*ERRγ*-luc) and then infected with either IAV or SARS-CoV-2 in the presence or absence of NAC. Both viruses significantly activated the *ERRγ* promoter and enhanced ERRγ expression, while NAC treatment attenuated this activation in both cases (Fig. 2c,d). We next investigated whether virus-induced ERRγ activation occurs through the JNK/c-Jun signaling pathway[26]. Notably, infection with either IAV or SARS-CoV-2 resulted in substantial phosphorylation of both JNK (p-JNK) and c-Jun (p-c-Jun) at 4 hpi and 8 hpi, respectively (Fig. 2e,f). Furthermore, a mutation in the c-Jun binding element AP1 on the *ERRγ* promoter (*ERRγ*-AP1mut-luc) significantly reduced *ERRγ*-luc activity in cells infected with either virus (Fig. 2g). Chromatin immunoprecipitation (ChIP) assays revealed that both viruses increased c-Jun occupancy at the AP1 regulatory element on the *ERRγ* promoter, an effect that was markedly blocked by NAC treatment (Fig. 2h,i). These data suggest that virus-induced ERRγ transactivation is primarily mediated through the ROS/JNK/c-Jun axis.

Virus-induced ERRγ transactivates SREBP-1c, leading to FA biosynthesis required for viral replication

In our previous studies, we established ERRγ as a transcriptional regulator of SREBP-1c, a crucial transcription factor that activates FA biosynthesis, and its dysregulation contributes to several fatty liver conditions[27]. To confirm whether ERRγ directly regulates the *SREBP-1c* transcription in virus-infected cells, we transfected cells with a luciferase reporter vector for the human *SREBP-1c* gene promoter (*SREBP-1c*-luc) and subsequently infected them with each target RNA virus. Infection with all seven target viruses significantly enhanced *SREBP-1c* promoter activity, comparable to the positive control of ERRγ overexpression (Flag-ERRγ) (Fig. 3a and Extended Data Fig. 4a). In contrast, mutating the ERR-response element (ERRE) from the *SREBP-1c* promoter (*SREBP-1c*-ERREmut-luc) led to a significant reduction in the activity. Treatment with the ERRγ inverse agonist DN200434 markedly suppressed *SREBP-1c* promoter activity (Fig. 3b and Extended Data Fig. 4b) and mRNA expression (Fig. 3c) in the cells infected with each virus. However, the basal level of *SREBP-1a* mRNA in SARS-CoV-2 or IAV-

infected cells was not influenced by the treatment with DN200434 (Extended Data Fig. 4c). These findings indicate that ERRγ directly transactivates the *SREBP-1c* gene in response to RNA viral infections.

We also observed that viral infections significantly increased the mRNA expression of lipogenic genes, including *FASN* (encoding fatty acid synthase), *DGAT1* (encoding diacylglycerol O-acyltransferase 1), and *SCD1* (encoding stearoyl-CoA desaturase 1) (Fig. 3d-f), leading to increased intracellular triacylglycerol (TAG) levels (Fig. 3g and Extended Data Fig. 4d). Treatment with DN200434 effectively attenuated both lipogenic gene activation and lipid accumulation in virus-infected cells (Fig. 3d-g). Notably, ERRγ haploinsufficiency in mice inhibited SREBP-1c activation, significantly reducing TAG accumulation and intracellular LD formation (Extended Data Fig. 4e,f).

To investigate the role of SREBP-1c in viral replication *in vivo*, we utilized whole-body *Srebp-1c* KO mice, with the KO condition confirmed by PCR genotyping and immunoblotting (Extended Data Fig. 5a,b). Notably, IAV-induced mortality in IAV-challenged WT mice was reduced from 100–25% in the *Srebp-1c* KO mice (Extended Data Fig. 5c). In addition, IAV-challenged *Srebp-1c* KO mice exhibited significant improvements in body weight loss and clinical scores, compared to WT IAV-infected mice (Extended Data Fig. 5d,e). *Srebp-1c* deficiency significantly reduced viral protein synthesis, genome replication, and progeny production, accompanied by a marked decrease in TAG level and LD formation (Extended Data Fig. 5f-j). Furthermore, IAV-infected *Srebp-1c* KO mice displayed reduced histopathological lung lesions, such as broncointerstitial pneumonia, along with substantially diminished viral replication in the cells of bronchioles and alveoli, compared to WT IAV-infected mice (Extended Data Fig. 5k).

Next, we investigated the impact of DN200434 treatment on the FFA profiles in virus-infected cells using a gas chromatography-flame ionization detector (GC-FID). A heatmap was generated based on selected FFAs that showed significant changes ($p < 0.05$) (Supplementary Tables 1 and 2). Interestingly, DN200434 treatment reduced the levels of FFAs chosen induced by SARS-CoV-2 or IAV infection to levels comparable to those of mock control cells (Fig. 3h,i), as confirmed by quantification of representative FFAs (Extended Data Fig. 6). To assess whether the supplementation of key FFAs might restore viral growth in DN200434-treated conditions, we selected four prominent FFAs: saturated palmitic acid (PA), monounsaturated oleic acid (OA), polyunsaturated linoleic acid (LA), and polyunsaturated arachidonic acid (AA)[13,16]. Supplementation of these individual FFAs restored genome replication and progeny production of SARS-CoV-2 and IAV in virus-infected, FFA-deprived cells, compared to inhibitor-treated controls (Fig. 3j-m). Taken together, these findings highlight the importance of the sequential pathway, beginning with ROS-induced activation of ERRγ, which transactivates *SREBP-1c*, promoting FA biosynthesis and subsequent LD accumulation, and demonstrate that pharmacological and genetic inhibition of the ERRγ/SREBP-1c axis effectively suppresses the FA anabolic pathway, which is essential for RNA viral replication.

Broad-spectrum antiviral activity of DN200434 in vitro

The studies so far suggest that targeting ERRγ might have a broad protective effect in limiting RNA virus replication. According to our previous lead compound optimization and pharmacokinetics studies,

DN200434 stands out as the most potent ERRγ inverse agonist, exhibiting a functional IC_{50} of 0.006 μM, which is 12-fold higher than the original lead compound GSK5182[28]. Importantly, DN200434 has displayed promising *in vitro*/*in vivo* toxicity profiles in the required standard discovery studies[28]. Thus, we comprehensively assessed the ERRγ inverse agonist DN200434 on the *in vitro* replication of seven target RNA viruses. We measured the half-maximal cytotoxic concentration (CC_{50}), half-maximal inhibitory concentration (IC_{50}), and selectivity index (SI). DN200434 showed IC_{50} values against the target RNA viruses at substantially lower micromolar concentrations than CC_{50} (Supplementary Tables 3 and 4, and Extended Data Fig. 7). Specifically, the IC_{50} values ranged from 1.89 ± 0.13 μM for SARS-CoV-2 to 6.42 ± 1.00 μM for PSaV. These results yielded significant SI values, with a 49 SI against SARS-CoV-2 and a 34 SI against IAV, highlighting the broad-spectrum antiviral potential of DN200434.

Mechanistically, DN200434 treatment significantly reduced SARS-CoV-2-induced perinuclear double-membrane vesicle (DMV) clusters containing viral double-stranded RNA, as evidenced by transmission electron microscopy (TEM) and confocal microscopy (Fig. 4a,b). TEM analysis further revealed a notable decrease in the number of progeny viral particles in DN200434-treated cells compared to vehicle-treated virus-infected cells (the lower two panels in Fig. 4a). Additionally, the palmitoylation of SARS-CoV-2 S protein and IAV HA proteins, typically observed in vehicle-treated, virus-infected cells, was significantly inhibited by DN200434 (Fig. 4c,d). Moreover, DN200434 treatment in SARS-CoV-2- and IAV-infected cells inhibited energy production via β-oxidation in the mitochondria using the FFA substrate (Fig. 4e).

SARS-CoV-2 and IAV infections induce significant mortality associated with a systemic inflammatory response, including a cytokine and eicosanoid storm, in patients with COVID-19 and influenza[29–33]. In the current study, treatment with DN200434 significantly reduced elevated levels of eicosanoids, such as leukotriene B4 (LTB4) and prostaglandin E_2 (PGE_2), derived from arachidonic acid in SARS-CoV-2- and IAV-infected cells (Fig. 4f,g). DN200434 also suppressed proinflammatory cytokines, including interferon-α (IFN-α), IFN-β, interleukin-6 (IL-6), tumor necrosis factor-α (TNF-α), and monocyte chemoattractant protein-1 (MCP-1) (Fig. 4h-l), which are typically activated in response to IAV infection[34]. In Vero cells, which lack IFN synthesis and are affected by SARS-CoV-2 proteins antagonizing types I and III IFNs[35,36], DN200434 significantly reduced TNF-α, IL-6, and MCP-1 levels, while IFN-α and IFN-β remained unchanged (Fig. 4h-l). These results suggest that DN200434 can mitigate the severe inflammatory response induced by viral infections, potentially reducing mortality in COVID-19 and IAV patients.

Antiviral activity of DN200434 against SARS-CoV-2 and IAV infection in vivo

To investigate the antiviral effect of DN200434 *in vivo*, hamsters were challenged with 10^5 $TCID_{50}$ of the SARS-CoV-2 KCDC03 strain. Intraperitoneal administration of DN200434, starting 12 h after the challenge and continuing for four and a half consecutive days (twice a day), significantly improved gross lung lesions in a dose-dependent manner on day 5. Notably, treatment with DN200434 at 40 mg kg^{-1} d^{-1} led to an impressive 92% reduction in gross lung lesions compared to the virus-challenged, vehicle-

treated control group (Fig. 5a,b). Virus replication was suppressed by the treatment with DN200434 in a dose-dependent manner (Fig. 5c,d). Treatment with DN200434 significantly decreased TAG levels, a major component of LDs, and reduced LDs in these cells in lung tissues compared to virus-challenged vehicle-treated controls (Fig. 5e,f). Importantly, DN200434-mediated inhibition of LD generation mitigated histopathological lung lesions (Fig. 5g, upper panels) and viral antigen distribution (Fig. 5g, lower panels). Furthermore, DN200434 significantly reduced levels of LTB4, PGE_2, IL-6, TNF-α, and MCP-1, without affecting IFN-α and IFN-β levels (Extended Data Fig. 8a-g). These results support the *in vitro* data showing that DN200434 has both antiviral and anti-inflammatory cytokine effects against SARS-CoV-2 infection.

Next, we evaluated the antiviral effects of DN200434 against the mouse-adapted IAV PR8 strain (H1N1) in mice. All IAV-challenged, vehicle-treated mice died within 10 days, while intraperitoneal DN200434 administration (twice daily for four days) improved survival rates, reaching 40% at 20 mg kg-1 d-1 (Fig. 5h,i). DN200434 also alleviated body weight loss and clinical scores associated with IAV infection (Fig. 5j,k). DN200434 treatment markedly reduced the presence of LDs and viral antigens within bronchial epithelial cells (Fig. 5l). This was accompanied by a significant decrease in TAG levels in lung tissues (Fig. 5m). Additionally, DN200434 effectively suppressed viral genome replication and progeny production (Fig. 5n,o). These antiviral effects corresponded with a notable reduction in histopathological lung lesions, such as interstitial thickening, alveolar and bronchiolar epithelial cell necrosis, and pulmonary edema (Fig. 5p). Furthermore, DN200434 significantly decreased the levels of inflammatory mediators, including LTB4, PGE_2, IFN-α, IFN-β, IL-6, TNF-α, and MCP-1 compared to virus-infected, vehicle-treated controls (Extended Data Fig. 8a-g).

In addition, we evaluated the antiviral effects of DN200434 combined with the SARS-CoV-2 RdRp-targeting remdesivir[37]. Hamsters were treated with 20 mg kg^{-1} d^{-1} DN200434 and/or 2.5 mg kg^{-1} d^{-1} remdesivir. Individually, DN200434 and remdesivir reduced gross lung lesions by 50% and 20%, respectively. Notably, combination therapy resulted in substantial reductions in gross lung lesions–80%, 75%, and 78%–in hamsters challenged with the KCDC03 strain (A lineage), KDCA51463 strain (alpha lineage), and KDCA55905 strain (beta lineage), respectively (Fig. 6a,b). Additionally, the combination therapy significantly mitigated body weight loss and improved clinical scores compared to monotherapies (Fig. 6c-e). Finally, we evaluated the synergistic antiviral effects of DN200434 in combination with oseltamivir, an IAV neuraminidase-targeting drug[37]. Mice received daily doses of 10 mg kg^{-1} DN200434 and 2 mg kg^{-1} oseltamivir. The combination therapy significantly improved outcomes, achieving a 90% survival rate in IAV-challenged mice (Fig. 6f,g). Additionally, the combined treatment effectively mitigated body weight loss associated with infection and provided superior relief of clinical symptoms compared to individual therapies (Fig. 6h,i). These findings highlight that combining the host-targeting DN200434 with virus-targeting drugs like remdesivir or oseltamivir produces synergistic antiviral effects. This approach demonstrates the therapeutic potential of concurrently targeting viral and host pathways to enhance efficacy against COVID-19 and IAV infections compared to monotherapies alone.

Discussion

Conventional antiviral drugs are typically designed to target viral proteins, often with high specificity for a single virus[7,38]. However, it is important to recognize that viruses extensively depend on an array of host proteins to orchestrate essential phases of their life cycles. Particularly noteworthy is the fact that many viruses share a reliance on common host proteins, making these proteins promising candidates for the development of host-directed antiviral agents with broad-spectrum efficacy[7,38]. In the present study, the target viruses included representatives of diverse RNA virus families, encompassing positive-stranded, negative single-stranded, and double-stranded genomes with linear or segmented arrangements within capsid or envelope structures; thus, they are representatives of a broad array of different major RNA viruses circulating in the past, current, and possibly future[39]. Interestingly, our study has discovered that DN200434 has broad-spectrum antiviral activity against different target viruses.

Mechanistically, we show that ROS-induced early activation of the JNK/c-Jun signaling pathway during IAV or SARS-CoV-2 infection drives increased ERRγ expression (Extended Data Fig. 9). Notably, treating virus-infected cells with the antioxidant NAC significantly suppressed the ERRγ activity, confirming its role as a ROS sensor in virus-infected cells[25]. Both IAV and SARS-CoV-2 infections triggered phosphorylation of JNK and c-Jun, directly activating the *ERRγ* promoter (Extended Data Fig. 9). Mutations in the AP1 regulatory element of the *ERRγ* promoter impede this activation. Moreover, NAC treatment significantly inhibited c-Jun binding to the AP1 site. These findings underscore the critical role of ROS-dependent JNK/c-Jun signaling in the induction and transactivation of ERRγ during viral infection (Extended Data Fig. 9).

We also demonstrate that ERRγ directly binds to an ERRE in the *SREBP-1c* gene promoter in RNA virus-infected cells, driving SREBP-1c-dependent FA biosynthesis (Extended Data Fig. 9). Interestingly, genetic and pharmacological inhibition of ERRγ significantly disrupted SREBP-1c-dependent FA biosynthesis, a process critical for efficient viral replication (Extended Data Fig. 9). This disruption impairs the formation of viral replication compartments (e.g., DMVs for SARS-CoV-2), viral morphogenesis (protein palmitoylation), and beta-oxidation-driven energy production[13,16]. Remarkably, supplementing four key FFAs restored viral replication in conditions of DN200434-induced FFA insufficiency, emphasizing the crucial role of ERRγ/SREBP-1c-mediated FA biosynthesis during viral infection[13,16].

The upsurge of proinflammatory cytokines, known as a cytokine storm, is critical in worsening pneumonia in COVID-19 and influenza patients, ultimately increasing severity and mortality[29,30]. In this study, both *in vitro* and *in vivo* inhibition of ERRγ with DN200434 significantly reduced eicosanoid and cytokine levels, pneumonia severity, and overall mortality compared to non-treated controls. This effect may involve two possible mechanisms. First, DN200434 suppresses the SREBP-1c-dependent FA biosynthesis, which could block the FA-derived eicosanoid or eicosanoid-associated cytokine storm[31]. Second, DN200434 impairs viral replication compartment formation, viral morphogenesis, and energy production, leading to reduced viral genomes and proteins, which may limit pathogen-associated

molecular patterns that would otherwise trigger a cytokine storm through pattern recognition receptors in the infected or immune cells[32]. These findings suggest that DN200434 could be a promising candidate for further investigation in clinical trials focused on severe pneumonia cases associated with COVID-19 and influenza.

Combination therapies offer an effective antiviral strategy by reducing toxicity and enhancing efficacy[37]. Antiviral agents typically operate through two main mechanisms: 1) targeting viral proteins or nucleic acids, and 2) targeting essential host factors involved in viral replication[40]. In this study, combination therapy with DN200434 and oseltamivir in IAV-infected mice, as well as DN200434 and remdesivir in SARS-CoV-2-infected hamsters, showed superior outcomes compared to vehicle and monotherapies, including reduced IAV-induced mortality and SARS-CoV-2-induced lung lesions, along with significant reductions in viral replication. Thus, future clinical trials should explore double or triple antiviral regimens incorporating DN200434 as a universal host-targeting agent[1–5,40].

In conclusion, we show that early ERRγ activation during RNA virus infections like SARS-CoV-2 and IAV drives SREBP-1c-dependent FA biosynthesis, establishing it as a broad-spectrum antiviral target. Treatment with DN200434, an ERRγ-specific inverse agonist significantly reduced viral replication by inhibiting this critical biosynthesis pathway, essential for viral replication, morphogenesis, and energy production. Furthermore, DN200434 alleviated lung lesions, viral replication, progeny production, and eicosanoid and proinflammatory cytokine levels in IAV- and SARS-CoV-2-infected cells or animals. These findings highlight the potential of an ERRγ inverse agonist as a broad-spectrum antiviral that modulates viral replication and cytokine storms.

Methods

Cells and viruses

Vero E6, MDCK, LLC-PK, MA104, A549, Caco-2, MARC-145, and HRT-18G cells were cultured in EMEM, α-MEM, or DMEM at 37°C in 5% CO_2. All the media were supplemented with 10% fetal bovine serum, 100 U/mL penicillin, and 100 μg/mL streptomycin. SARS-CoV-2 (KCDC03, KDCA51463, and KDCA55905 strains), IAV [PR8/34 (H1N1) strain], BCoV (KWD20 strain), PEDV (QIAP1401 strain), PRRSV (LYM strain), RVA (NCDV strain), and PSaV (Cowden strain) were used in this study. Detailed procedures for cell and virus culture, as well as virus titration, are provided in the Supplementary Information.

Chemicals, kits, siRNAs, and antibodies

The details of the reagents, antibodies, siRNAs, and kits used in this study are provided in the Supplementary Information.

Plasmids, transfection, and luciferase-based assay

We used plasmids that contained various gene promoters fused to the luciferase gene, including the human SREBP-1c gene promoter (*SREBP-1c*-luc), a mutant version of the human *SREBP-1c* ERR-response element (ERRE) gene promoter (*SREBP-1c* ERREmut-luc), the human *ESRRG* gene promoter (*ERRγ*-luc), and a site-specific AP1 mutant version of the human *ESRRG* gene promoter (*ERRγ*-AP1mut-luc), and the human *ESRRG* gene fused to a flag-tag in the pcDNA3.0 backbone (encoding Flag-ERRγ). These constructs were transfected as previously described[11,26,27]. Supplementary Information contains comprehensive procedures.

Cytotoxicity assessment

The half-maximal cytotoxic concentration (CC_{50}) of the chemicals and their solvents was determined using the MTT assay, whose procedure is described in Supplementary Information.

Treatment of cells with inhibitory chemicals and FFAs

The above cell lines grown in 6- or 12-well plates or 8-well chamber slides with the desired confluency were washed twice with phosphate-buffered saline (PBS, pH 7.4). Thereafter, they were then mock-inoculated with medium only or inoculated with the virus at the following multiplicities of infection (MOI): MOI of 1 or 0.1 FFU of SARS-CoV-2, IAV, BCoV, PEDV, PRRSV, and PSaV. After absorbing each inoculum for 1 h, the cells were washed twice with PBS (pH 7.4). Cells were treated with DN200434 (at 1 μM, 10 μM, or 20 μM concentration) or vehicle immediately following virus absorption and incubated for the indicated time. For virus recovery experiments, cells treated with DN200434 after infections with IAV or SARS-CoV-2 were supplied with PA, OA, LA, or AA at 100 μM concentration and incubated further for the indicated periods. Each cell lysate and the supernatant were used for the different experiments, as described below. More details are described in the Supplementary Information.

The preparation of fatty acid methyl esters (FAMEs) from the cells

The FFAs in mock-, IAV-infected A549, and SARS-CoV-2-infected Vero E6 cells that were either DN200434- or vehicle-treated underwent saponification, methylation, and extraction as described in detail in the Supplementary Information in detail.

Gas chromatography-flame ionization detector (GC-FID) analysis of FAMEs

The composition of FFAs in mock-infected, IAV-infected, and SARS-CoV-2-infected cells was analyzed by GC-FID analysis of fatty acid methyl esters (FMEs). The detailed procedure is provided in the Supplementary Information.

LC-MS to quantify fatty acids

The amount of palmitic acid (PA), oleic acid (OA), linoleic acid (LA), arachidonic acid (AA), stearic acid (SA), and eicosenoic acid (EA) in untreated and treated cells after infection with IAV or SARS-CoV-2 was determined by LC-MS, as described previously[13].

Heatmap cluster graphs

According to GC-MS analysis, a heatmap was created using R software (version 4.3.1). The rows are mock- or virus-infected groups with either vehicle or DN200434 treatment, and the columns are the target fatty acids, as previously described[41]. Detailed procedures are described in Supplementary Information.

Chromatin immunoprecipitation (ChIP) assay

ChIP assay was carried out according to previous studies[11,27]. After recovering DNA, qPCR was performed using primers spanning the AP1-binding region on the human *ESRRG* gene promoter as described in Supplementary Information.

Determination of fatty acid oxidation (FAO)

FAO activity, either in vehicle-treated or DN200434-treated cells, was determined using a colorimetric FAO assay kit (AssayGenie), as described in the Supplementary Information.

Ethics statement

All animal experiments were performed in strict accordance with the institutional animal care and use committees' requirements at Chonnam National University (CNU IACUC-YB-2023-20) and Korea Research Institute of Bioscience & Biotechnology (KRIBB-AEC-22043, KRIBB-IBC-20220203). All animals were treated following the international laws and policies outlined in the NIH Guide for the Care and Use of Laboratory Animals, NIH Publication No. 85 – 23 (1985), revised in 1996. All experiments were carried out in a way that reduced the number of animals required and minimized their suffering.

Experimental animals

Supplementary Information describes the species, breed, acclimation, and preparation of the animals used in this study.

Measurement of proinflammatory and eicosanoids cytokines in the cell culture supernatant and bronchoalveolar lavage fluid (BALF)

Proinflammatory cytokines such as IFN-α, IFN-β, TNF-α, IL-6, and MCP-1 and eicosanoids such as LTB4 and PGE_2 were measured in the supernatant of IAV-infected A549 or SARS-CoV-2-infected Vero E6 cells or from bronchioalveolar lavage fluid from IAV-challenged mice or SARS-CoV-2-challenged hamsters as described in Supplementary Information.

Determination of median lethal dose (LD_{50}) of mouse-adapted PR8 strain

The LD_{50} of the mouse-adapted A/PR8/34 (H1N1) strain was obtained as described in the protocols in Supplementary Information.

In vivo antiviral activity, lipid metabolism, and pathogenicity

Antiviral effects of DN200434, either singly or in combination with oseltamivir against IAV infection or remdesivir against SARS-CoV-2 infection, were carried out in mouse and hamster models, respectively, as described in Supplementary Information.

Plaque assay

A plaque assay was performed to determine the IAV titer as described in Supplementary Information.

Median Tissue culture infectious dose ($TCID_{50}$) assay

$TCID_{50}$ assay was performed to determine the SRAS-CoV-2 titer as described in Supplementary Information.

Immunofluorescence assay (IFA)

IFA evaluated the dynamics of ERRγ, SREBPs, and LD, viral replication, and infectivity in cultured cells or lung tissue. In addition, the effect of gene knockout or knockdown was measured using IFA, as described in Supplementary Information.

Western blot analysis

Western blot analysis was used to detect target cellular or viral proteins in the cultured cells or lung tissues. Normalization and graphic representation were carried out in compliance with the protocols in the Supplementary Information.

Triglyceride colorimetric assay

A triglyceride colorimetric kit was used to measure intracellular TAGs as described in Supplementary Information.

Quantitative real-time PCR

Real-time PCR was conducted to detect and quantify the target viral RNAs and host mRNAs from cultured cells or animals according to the procedures described in Supplementary Information.

Palmitoylation assay

The effect of DN200434 on palmitoylation of SARS-CoV-2 S protein or IAV HA in virus-infected cells was measured by palmitoylation assay CAPTUREome™ S-palmitoylated protein kit (Badrilla) as described in Supplementary Information.

Transmission electron microscopy (TEM)

Ultrastructural evaluation of double-membrane vesicles (DMVs) in SARS-CoV-2-infected cells was performed by TEM as described elsewhere[42], and its procedure is described in Supplementary Information.

Histopathology

Histopathological changes were analyzed in IAV-infected mice or SARS-CoV-2-infected hamsters as described in Supplementary Information.

Immunohistochemistry (IHC)

Antibody-mediated evaluation on IAV or SARS-CoV-2 proteins from experimental animals was carried out according to the protocols provided in Supplementary Information.

Illustrations

Illustrations of animals (mouse and hamster) were created with BioRender software (https://biorender.com/).

Declarations

Data availability

The main data supporting this study's findings are available in the article and its Supplementary Information section. The corresponding authors provide additional source data underlying the figures featured in the Supplementary Notes upon request. Source data are provided with this paper.

Competing interests

K.-O.C. and D.J.L. are board members of Pharmacolinx, and H.-Y.J. and I.-K.L. are board members of NovMetaPharma. All other authors declare that they have no competing interests.

Correspondence and requests for materials

should be addressed to Kyoung-Oh Cho (email: choko@jun.ac.kr), Hueng-Sik Choi (email: hsc@jnu.ac.kr), Don-Kyu Kim (dkkim2@jnu.ac.kr), and Tae-Il Jeon (tjeon@jnu.ac.kr).

Author contributions

Y.-B.B, H.-J.K, T.-I. J D.-K.K, H.-S.C, and K.-O.C conceived and designed the experiments; Y.-B.B and H.-J.K performed the majority of the experiments, including *in vitro* and *in vivo* antiviral experiments; H.-J.J, S.-H.J, I.-C.L, and Y.-B.R. performed GC-FID, LC-MS, and heatmap analysis; M.S., T.H.N., and M.J.A. participated *in vitro* and *in vivo* antiviral experiments; Y.-B.B, H.-J.K., D.-K.K, B.C., W.-R.P., M.J.A., J.-G.P., I.-S.S, E.K., C.M., H.-Y.J, I.-K.L, T.-I.J, H.-S.C, and K.-O.C. analyzed the silencing effects of target genes in response to *in vitro* and *in vivo* virus infections; D.-K.K, J.-G.P., I.-S.S., E.K., C.M., J.-S.K., S.-S.L., H.-E.C., H.-Y.J, I.-K.L., H.-Y.J, D.J.L, T.F.O., T.-I.J, H.-S.C, and K.-O.C. provided theoretical contributions to the project; Y.-B.B, H.-J.K., T.-I. J, D.-K.K, H.-S.C, and K.-O.C. analyzed the data and wrote the manuscript.

Acknowledgments

We thank Professor U. Desselberger at the Department of Medicine, University of Cambridge, for critical reading and discussion. This work was supported by the National Research Foundation of Korea (NRF) grant funded by the Korean government (MSIT) (RS-2023-00219517, RS-2024-00339845, RS-2024-00342230, RS-2021-NR058898, RS-2021-NR058546) and the KRIBB Research Initiative Program (KGM 5242221), which are funded by the Ministry of Science, ICT and Future Planning, Republic of Korea.

References

1. Baker RE et al (2022) Infectious disease in an era of global change. Nat Rev Microbiol 20:193–205
2. Caserta LC et al (2024) Spillover of highly pathogenic avian influenza H5N1 virus to dairy cattle. Nature 634:669–676
3. Eisfeld AJ et al (2024) Pathogenicity and transmissibility of bovine H5N1 influenza virus. Nature 633:426–432
4. Novella IS, Presloid JB, Taylor RT (2014) RNA replication errors and the evolution of virus pathogenicity and virulence. Curr Opin Virol 9:143–147
5. Meganck RM, Baric RS (2021) Developing therapeutic approaches for twenty-first-century emerging infectious viral diseases. Nat Med 27:401–410
6. Wu X et al (2017) Progress of small molecular inhibitors in the development of anti-influenza virus agents. Theranostics 7:826–845
7. Tripathi D, Sodani M, Gupta PK, Kulkarni S (2021) Host directed therapies: COVID-19 and beyond. Curr Res Pharmacol Drug Discov 2:100058
8. Miller MS, Mymryk JS (2011) An unhealthy relationship: viral manipulation of the nuclear receptor superfamily. Future Microbiol 6:999–1019
9. Misra J, Kim DK, Choi HS (2017) ERRγ: a Junior Orphan with a Senior Role in Metabolism. Trends Endocrinol Metab 28:261–272

10. Crevet L, Vanacker JM (2020) Regulation of the expression of the estrogen related receptors (ERRs). Cell Mol Life Sci 77:4573–4579
11. Kim DK et al (2014) Inverse agonist of estrogen-related receptor γ controls Salmonella typhimurium infection by modulating host iron homeostasis. Nat Med 20:419–424
12. Levy G et al (2016) Nuclear receptors control pro-viral and antiviral metabolic responses to hepatitis C virus infection. Nat Chem Biol 12:1037–1045
13. Baek YB et al (2022) Therapeutic strategy targeting host lipolysis limits infection by SARS-CoV-2 and influenza A virus. Signal Transduct Target Ther 7:367
14. Ketter E, Randall G (2019) Virus Impact on Lipids and Membranes. Annu Rev Virol 6:319–340
15. Monson EA, Trenerry AM, Laws JL, Mackenzie JM, Helbig KJ (2021) Lipid droplets and lipid mediators in viral infection and immunity. FEMS Microbiol Rev 45
16. Yuan S et al (2019) SREBP-dependent lipidomic reprogramming as a broad-spectrum antiviral target. Nat Commun 10:120
17. Laufman O, Perrino J, Andino R (2019) Viral Generated Inter-Organelle Contacts Redirect Lipid Flux for Genome Replication. Cell 178:275–289e216
18. Monson EA et al (2021) Intracellular lipid droplet accumulation occurs early following viral infection and is required for an efficient interferon response. Nat Commun 12:4303
19. Meng Z, Liu Q, Sun F, Qiao L (2019) Hepatitis C virus nonstructural protein 5A perturbs lipid metabolism by modulating AMPK/SREBP-1c signaling. Lipids Health Dis 18:191
20. Petersen J et al (2014) The major cellular sterol regulatory pathway is required for Andes virus infection. PLoS Pathog 10:e1003911
21. Wang L et al (2018) CVB3 Nonstructural 2A Protein Modulates SREBP1a Signaling via the MEK/ERK Pathway. J Virol 92
22. Cardelli M, Aubin JE (2014) ERRγ is not required for skeletal development but is a RUNX2-dependent negative regulator of postnatal bone formation in male mice. PLoS ONE 9:e109592
23. Laforge M et al (2020) Author Correction: Tissue damage from neutrophil-induced oxidative stress in COVID-19. Nat Rev Immunol 20:579
24. Paiva CN, Bozza MT (2014) Are reactive oxygen species always detrimental to pathogens? Antioxid Redox Signal 20:1000–1037
25. Vernier M et al (2020) Estrogen-related receptors are targetable ROS sensors. Genes Dev 34:544–559
26. Kim DK et al (2013) Estrogen-related receptor γ controls hepatic CB1 receptor-mediated CYP2E1 expression and oxidative liver injury by alcohol. Gut 62:1044–1054
27. Kim DK et al (2019) Estrogen-related receptor γ controls sterol regulatory element-binding protein-1c expression and alcoholic fatty liver. Biochim Biophys Acta Mol Cell Biol Lipids 1864:158521
28. Singh TD et al (2019) A Novel Orally Active Inverse Agonist of Estrogen-related Receptor Gamma (ERRγ), DN200434, A Booster of NIS in Anaplastic Thyroid Cancer. Clin Cancer Res 25:5069–5081

29. Mehta P et al (2020) COVID-19: consider cytokine storm syndromes and immunosuppression. Lancet 395:1033–1034
30. Ye Q, Wang B, Mao J (2020) The pathogenesis and treatment of the `Cytokine Storm' in COVID-19. J Infect 80:607–613
31. Hammock BD, Wang W, Gilligan MM, Panigrahy D (2020) Eicosanoids: The Overlooked Storm in Coronavirus Disease 2019 (COVID-19)? Am J Pathol 190:1782–1788
32. Takeuchi O, Akira S (2010) Pattern recognition receptors and inflammation. Cell 140:805–820
33. Wilkins C, Gale M (2010) Jr. Recognition of viruses by cytoplasmic sensors. Curr Opin Immunol 22:41–47
34. Gu Y et al (2021) The Mechanism behind Influenza Virus Cytokine Storm. Viruses 13
35. Desmyter J, Melnick JL, Rawls WE (1968) Defectiveness of interferon production and of rubella virus interference in a line of African green monkey kidney cells (Vero). J Virol 2:955–961
36. Zheng Y et al (2020) Severe acute respiratory syndrome coronavirus 2 (SARS-CoV-2) membrane (M) protein inhibits type I and III interferon production by targeting RIG-I/MDA-5 signaling. Signal Transduct Target Ther 5:299
37. Hung IF et al (2020) Triple combination of interferon beta-1b, lopinavir-ritonavir, and ribavirin in the treatment of patients admitted to hospital with COVID-19: an open-label, randomised, phase 2 trial. Lancet 395:1695–1704
38. Kausar S et al (2021) A review: Mechanism of action of antiviral drugs. Int J Immunopathol Pharmacol 35:20587384211002621
39. Payne S (2017) Introduction to RNA Viruses. Viruses, 97–105
40. Rayner CR et al (2020) Accelerating Clinical Evaluation of Repurposed Combination Therapies for COVID-19. Am J Trop Med Hyg 103:1364–1366
41. Santamaría R, Therón R, Quintales L (2008) BicOverlapper: a tool for bicluster visualization. Bioinformatics 24:1212–1213
42. Twu WI et al (2021) Contribution of autophagy machinery factors to HCV and SARS-CoV-2 replication organelle formation. Cell Rep 37:110049

Figures

Figure 1.

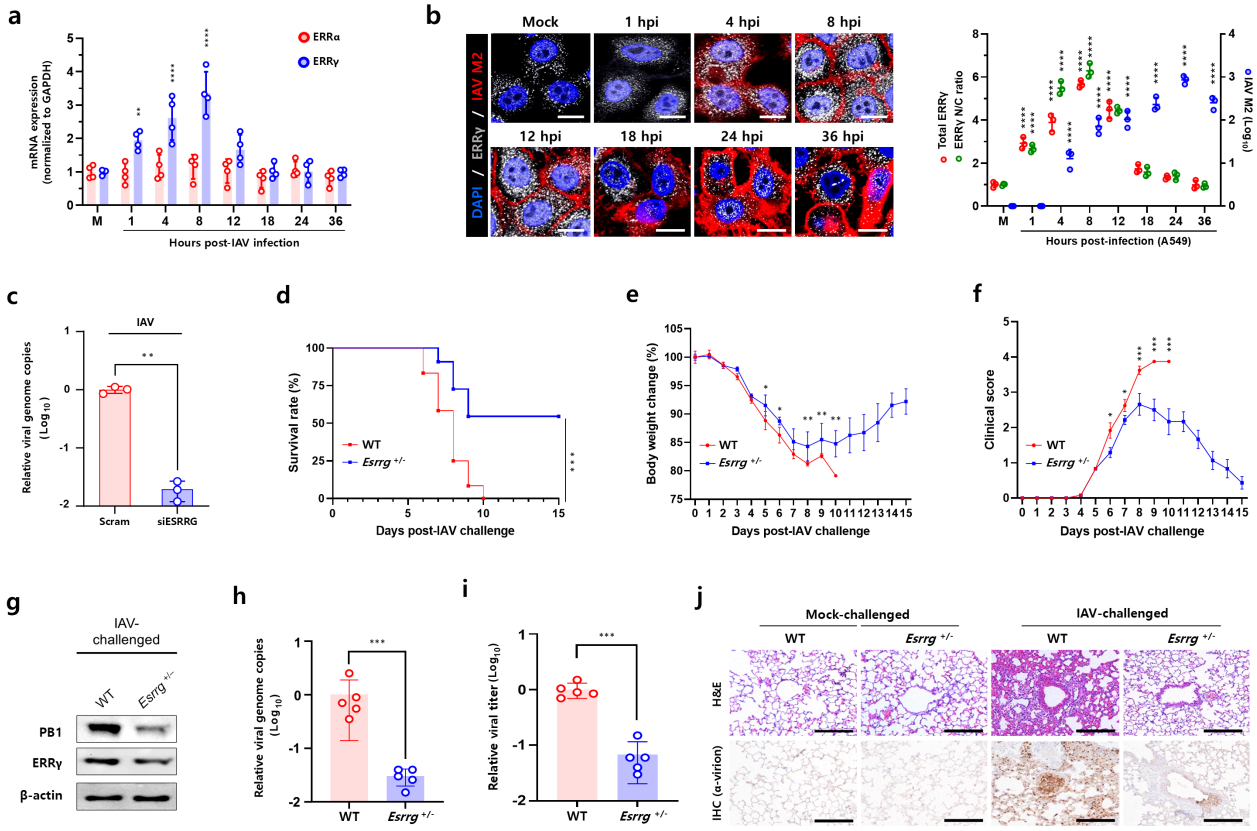

Figure 1

ERRγ is required for viral replication *in vitro* and *in vivo*.

a Quantification of transcription levels of *ERRa* and *ERRγ* genes in A549 cells infected with IAV PR8 strain at an MOI of 1 FFU, which are determined by RT-qPCR analysis. **b** Representative confocal images (left) and quantification (right) of sequential changes of ERRγ (white) and IAV M2 protein (red) in the cytoplasm and nucleus of A549 cells infected with IAV PR8 strain at an MOI of 1 FFU. Scale bars = 10 μm. **c** Reduction in IAV genome copy number by silencing of ERRγ. **d-f** Comparison of survival rates (**d**), body weight changes (**e**), and clinical scores (**f**) between wild-type (WT) and *Esrrg*$^{+/-}$ mice after challenge with 10^3 PFU of the mouse-adapted IAV PR8 strain (n = 16). **g-i** Comparison of levels of IAV PB1 protein (**g**), viral genome copy (**h**), and viral titer (**i**) in the lungs from WT and *Esrrg*$^{+/-}$ mice after challenge with 10^3 PFU of the mouse-adapted IAV PR8 strain (n = 5). **j** Representative images of histological lesion changes (upper panels) and immunohistochemical changes (lower panels) of viral antigen distribution in the lungs from the WT or *Esrrg*$^{+/-}$ mice after challenge with 10^3 PFU of the mouse-adapted IAV PR8 strain. Scale bars = 800 μm. All data in the graphs are presented as arithmetic means ± S.D. from three independent experiments. For statistical analysis, a one-way analysis of variance was carried out with Tukey's correction for multiple comparisons. *P < 0.05, **P < 0.01, ***P < 0.001, ****P < 0.0001.

Figure 2

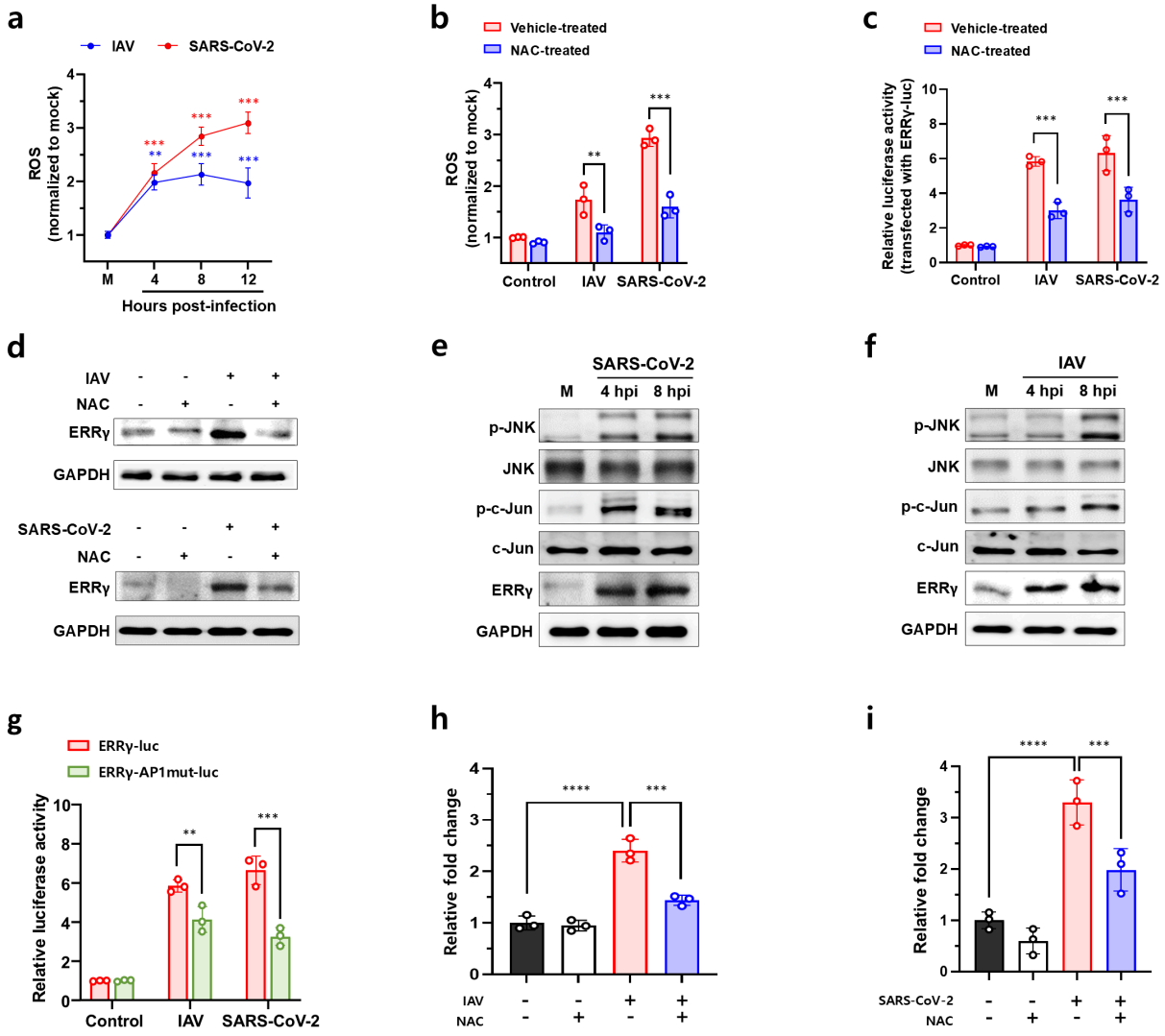

Figure 2

Transactivation of ERRγ in virus-infected cells through ROS/JNK/c-Jun axis.

a ROS levels in SARS-CoV-2-infected Vero E6 cells (MOI = 0.1 FFU) and IAV-infected A549 cells (MOI = 1 FFU) at different time points, which are normalized to a mock-infected control. **b** Reduction in the ROS levels in IAV-infected A549 cells or SARS-CoV-2-infected Vero E6 cells by treatment with N-acetylcysteine (NAC) antioxidant. **c** Reduction in luciferase activity by treatment with the N-acetylcysteine (NAC) antioxidant in IAV-infected A549 cells or SARS-CoV-2-infected Vero E6 cells, both containing a plasmid with the full-length of *ERRγ*promoter-luciferase gene (*ERRγ*-luc). **d** Reduction in ERRγ expression by treatment with the NAC in IAV- and SARS-CoV-2-infected cells. GAPDH was used as a loading control. **e, f** Phosphorylation of JNK and c-Jun in response to infection with SARS-CoV-2 (**e**) or IAV (**f**). GAPDH was used as a loading control. **g** Lesser activation of site-specific AP1 mutant *ERRγ*promoter (*ERRγ*-AP1mut-

luc) than full-length *ERRγ* promoter (*ERRγ*-luc) by infection with IAV and SARS-CoV-2. **h, i** Chromatin immunoprecipitation assay. Marked reduction in IAV- (**h**) and SARS-CoV-2-mediated occupancy (**i**) of c-Jun on the AP1 regulatory element site of *ERRγ*promoter by treatment with NAC. All data in the graphs are presented as arithmetic means ± S.D. from four independent experiments. A one-way analysis of variance was carried out with Tukey's correction for multiple comparisons. **P* < 0.05, ***P* < 0.01, ****P* < 0.001, *****P* < 0.0001.

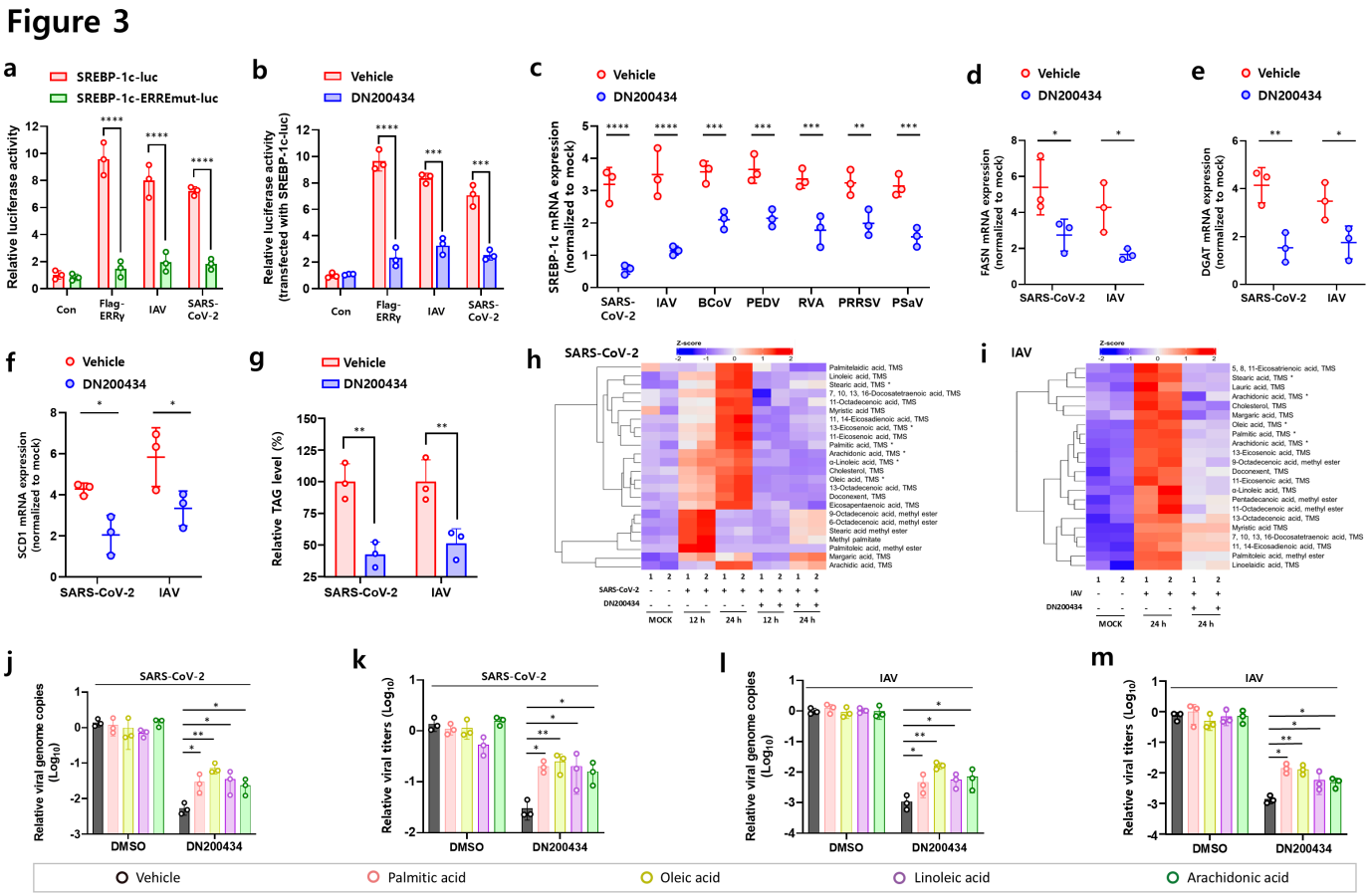

Figure 3

Virus-induced ERRγ upregulates fatty acid synthesis by inducing SREBP-1c expression.

a An ERRE-dependent activation of *SREBP-1c* promoter in IAV- or SARS-CoV-2-infected cells. Cells transfected with either *SREBP-1c*-luc or *SREBP-1c*-ERREmut-luc plasmid were left mock-infected, transfected with pcDNA3.0-Flag-ERRγ (encoding Flag-ERRγ), or infected with IAV at an MOI of 2 FFU or SARS-CoV-2 at an MOI of 2 FFU. **b**Treatment with DN200434, an inverse agonist of ERRγ, inhibited ERRE-dependent activation of the *SREBP-1c* promoter in IAV- or SARS-CoV-2-infected cells. Cells transfected with *SREBP-1c*-luc were left mock-infected, transfected with Flag-ERRγ, or infected with either IAV (MOI = 2 FFU) or SARS-CoV-2 (MOI = 2 FFU), and then treated with DN200434 at 20 μM. **c**The blockade of ERRγ by treatment with its inverse agonist DN200434 at a concentration of 20 μM inhibited the transcriptional activity of its target *SREBP-1c*gene in cells individually infected with each target virus. **d-f** RT-qPCR

analysis of mRNA of genes involved in fatty acid biosynthesis. Inhibition of ERRγ by the treatment with DN200434 at 20 μM concentration blocked the mRNA expression of *FASN*(**d**), *DGAT* (**e**), and *SCD1* (**f**) compared to vehicle-treated control. **g** Inhibition of ERRγ by the treatment with 20 μM of DN200434 reduced the formation of triacylglyceride (TAG) in the cells compared to mock-treated controls. **h, i** Heatmaps showing the changes in fatty acids following treatment of SARS-CoV-2-infected Vero E6 cells (MOI = 0.1 FFU) and IAV-infected A549 cells (MOI = 1 FFU) with DN200434. The cells were mock-infected or infected with the above virus and treated with vehicle or 20 μM of DN200434. A higher intensity of fatty acid in the rectangle than normal is indicated in red, and a lower is indicated in blue. TMS, trimethylsilyl ester. *, Representative fatty acids for further analysis. **j-m**Increase in viral genome copy and progeny numbers of SARS-CoV-2 (**j** and **k**) and IAV (**l** and **m**) through individual supplementation of exogenous palmitic, oleic, linoleic, or arachidonic acids in the above FFA-deprived condition. All data in the graphs are presented as arithmetic means ± S.D. from four independent experiments. *$P < 0.05$; **$P < 0.01$; ***$P < 0.001$, ****$P < 0.0001$, a one-way analysis of variance with Tukey's correction for multiple comparisons.

Figure 4

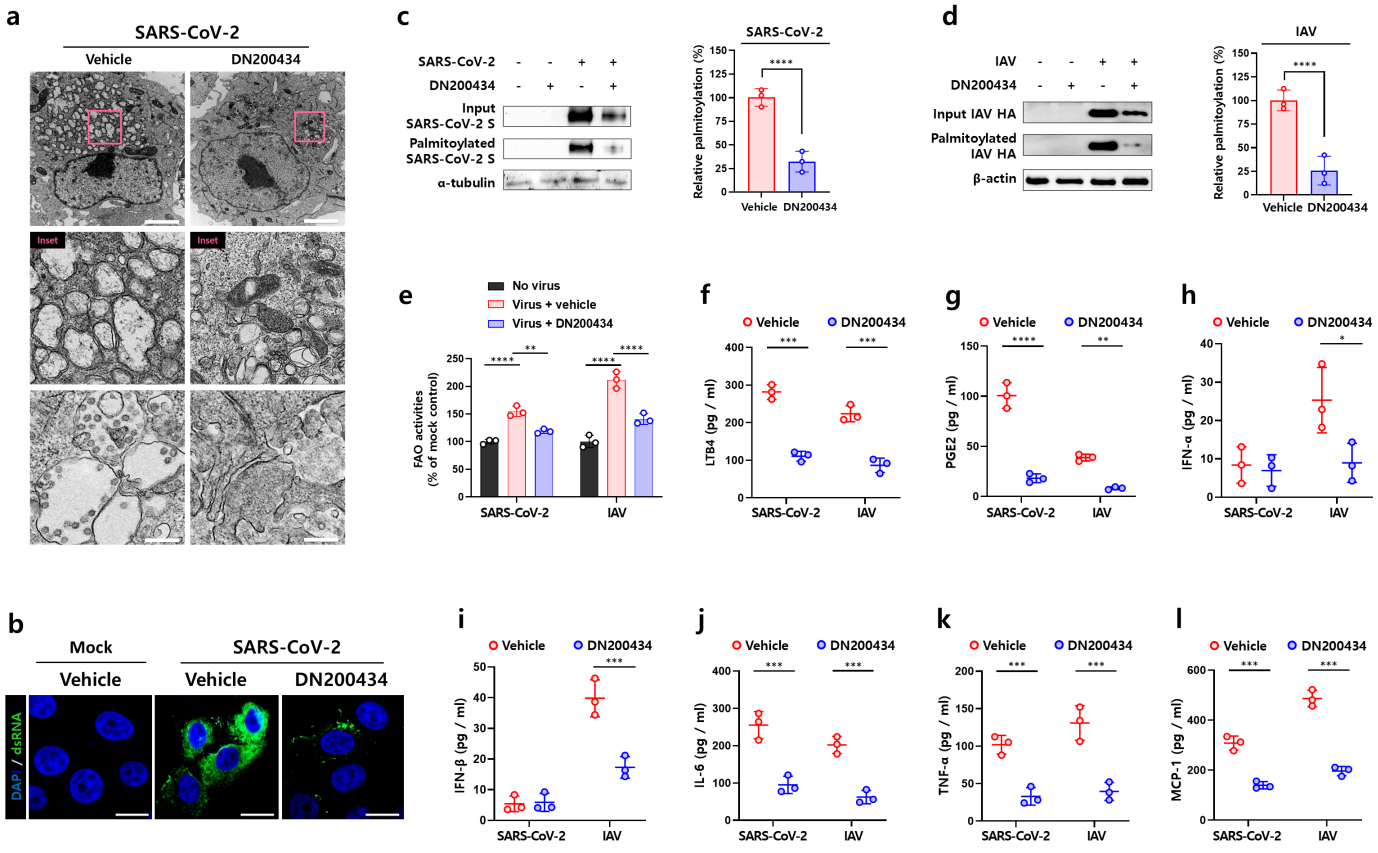

Figure 4

Antiviral and anti-inflammatory effects of DN200434 *in vitro*.

a Inhibition of double-membrane vesicle (DMV) formation in the SARS-CoV-2-infected cells (MOI = 0.1 FFU) by the treatment with DN200434. Note relatively few perinuclear double-membrane vesicles (upper

and middle panels) or virus particles (lower panel) in the DN200434-treated cells compared to vehicle-treated control cells. Scale bars: upper panels, 3 μm; lower panels, 300 nm. **b** Inhibition of double-stranded RNA (dsRNA) formation in the SARS-CoV-2-infected cells by the treatment with DN200434. Note the relatively small amount of dsRNA-positive fluorescence signals in the DN200434-treated cells compared to vehicle-treated control cells. Scale bars = 10 μm. **c, d** Representative western blot (left) and quantification (right) of inhibitory effects of DN200434 on palmitoylations of S protein in SARS-CoV-2-infected cell (MOI = 0.1 FFU, **c**) and HA protein in IAV-infected cells (MOI = 1 FFU, **d**) at 36 hpi and 24 hpi, respectively. **e** Graphical representation of inhibitory effects of DN200434 on intracellular fatty acid oxidation (FAO) activities in the SARS-CoV-2-infected cells (MOI = 0.1 FFU) and IAV-infected cells (MOI = 1 FFU) at 36 hpi and 24 hpi, respectively. **f-l** The graphical representation of the LTB4 (**f**), PGE_2 (**g**), IFN-α (**h**), IFN-β (**i**), IL-6 (**j**), TNF-α (**k**), and MCP-1 (**l**) levels in SARS-CoV-2-infected Vero E6 cells (MOI = 0.1 FFU) and IAV-infected A549 cells (MOI = 1 FFU), which were vehicle-treated or treated with DN200434. Each eicosanoid and cytokine level was determined by ELISA assay as described in the Materials and Methods section. Results are presented as arithmetic means ± S.D. **P* < 0.05; ***P* < 0.01; ****P* < 0.001, *****P* < 0.0001, a one-way analysis of variance with Tukey's correction for multiple comparisons.

Figure 5

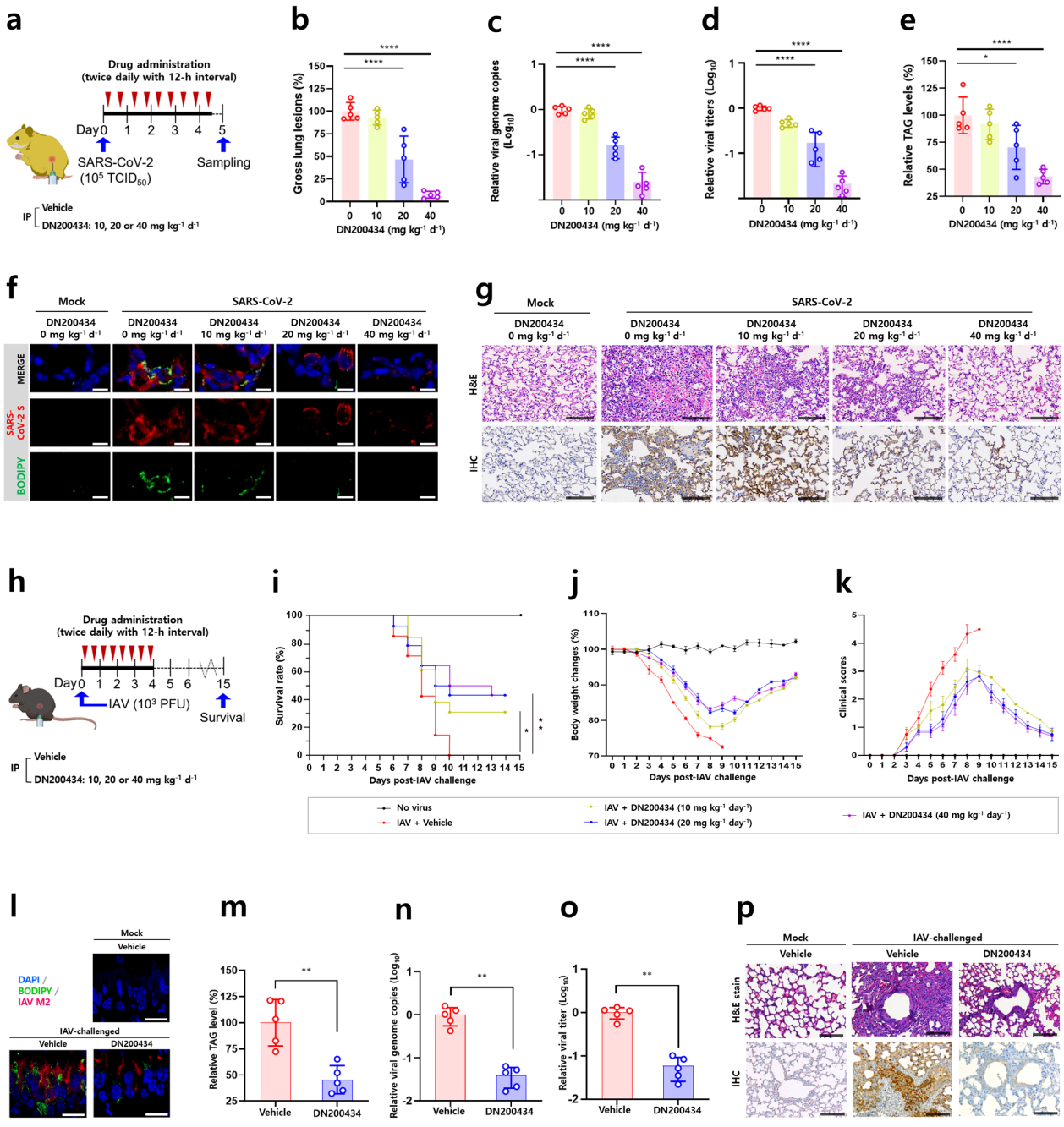

Figure 5

Antiviral effects of DN200434 against SARS-CoV-2 and IAV *in vivo*.

a Scheme of chemical administration twice daily for four and a half consecutive days after challenge with 10^5 $TCID_{50}$ of SARS-CoV-2 KCDC03 strain to Syrian hamsters (n = 5). **b** Reduction in SARS-CoV-2-induced gross lung lesions in hamsters by treatment with DN200434. **c-e** Graphical representation of

dose-dependent reduction in viral genome copy numbers (**c**), infectious progeny titers (**d**), and triacylglyceride (**e**) in lungs sampled from SARS-CoV-2-challenged hamsters (n = 5) by treatment with DN200434. **f** Representative images of dose-dependent reduction in BODIPY-stained LDs (green, lower panels) and inhibition of SARS-CoV-2 replication (red, middle panels) in alveolar pneumocytes of lung tissues sampled from SARS-CoV-2-challenged hamsters by treatment with DN200434. **g** Representative images of histological lesion changes (upper panels) and SARS-CoV-2-antigen distribution (lower panels) appeared by either hematoxylin and eosin stain (H&E) or immunohistochemistry (IHC) in the lungs. **h** Scheme of chemical administration twice daily for four consecutive days after challenge with 10^3 PFU of mouse-adapted IAV PR8 strain to mice (n = 16). **i-k** Comparison of survival rates (**i**), body weight changes (**j**), and clinical scores (**k**) in each experimental condition. **l** Representative confocal images of dose-dependent reduction in BODIPY-stained LDs (green) and inhibition of IAV replication (red) in bronchiolar epithelial cells of lung tissues sampled from IAV-challenged mice by treatment with DN200434. **m-o** Graphical representation of dose-dependent reduction in TAG (**m**), viral genome copy numbers (**n**), and infectious progeny titers (**o**) in lungs sampled from IAV-challenged mice (n = 5) by treatment with DN200434. **p** Representative images of histological lung lesions (upper panels) and immunohistochemical antigen distribution of IAV (lower panels). Results are presented as arithmetic means ± S.D. *P < 0.05; **P < 0.01; ***P < 0.001, ****P < 0.0001, a one-way analysis of variance with Tukey's correction for multiple comparisons. Scale bars = 10 μm for panels **f** and **l** and 800 μm for panels **g** and **p**.

Figure 6

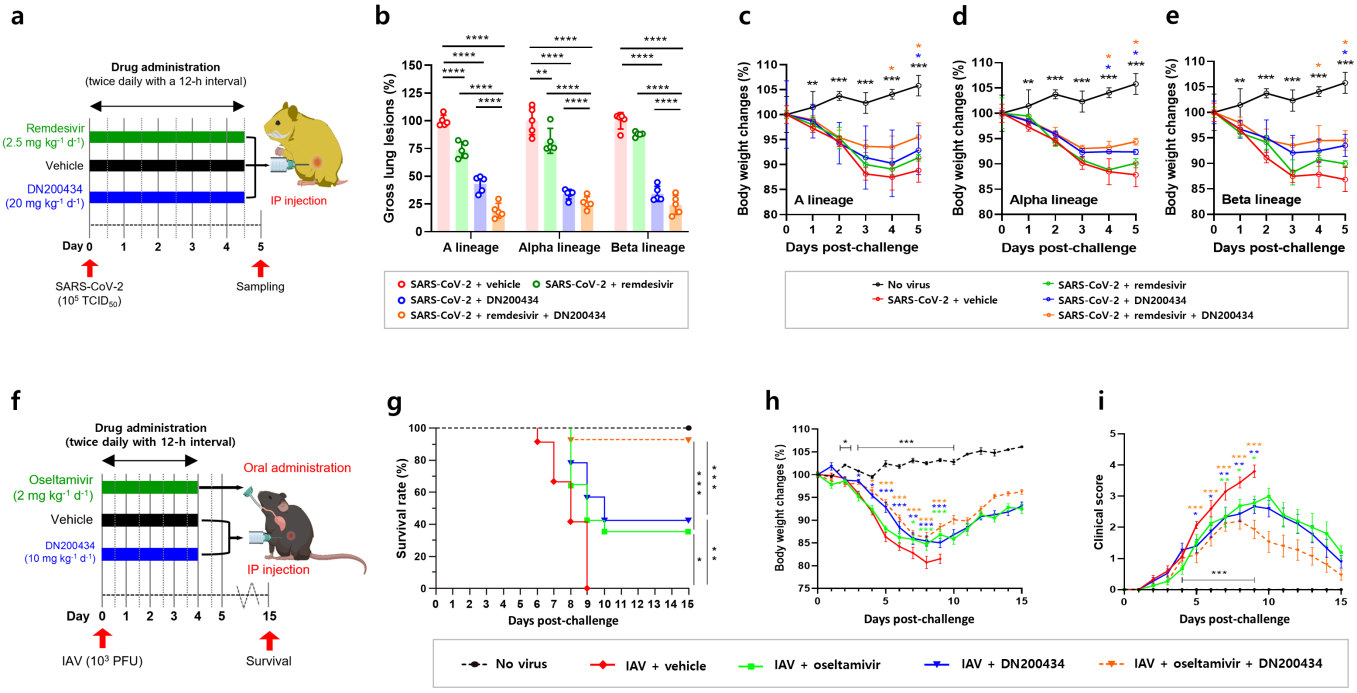

Figure 6

a Scheme of chemical administration of DN200434 and remdesivir, either individually or in combination, twice daily for four and a half consecutive days after challenge with 10^5 $TCID_{50}$ of SARS-CoV-2 KCDC03

(closely related to early Chinese strains), KDCA51463 (Alpha lineage with British variants), and KDCA55905 (Beta lineage with South African variants) to Syrian hamsters (*n* = 5). **b** Reduction in gross lung lesions in Syrian hamsters challenged with each strain by combination therapy with DN200434 and remdesivir. **c-e** Effect of treatments on the recovery of body weight in SARS-CoV-2 KCDC03 strain-challenged (**c**), KDCA51463 strain-challenged (**d**), and KDCA55905 strain-challenged (**e**) groups. **f** Scheme of chemical administration of DN200434 and oseltamivir, either individually or in combination, twice daily for four consecutive days after challenge with 10^3 PFU of mouse-adapted IAV PR8 strain to mice (*n* = 16). **g-h** Effect of treatments on survival rates (expressed as percentages) (**g**), body weight changes (**h**), and clinical scores (**i**) in each group. Results are presented as arithmetic means ± S.D. **P* < 0.05; ***P* < 0.01; ****P* < 0.001, *****P* < 0.0001, a one-way analysis of variance with Tukey's correction for multiple comparisons.

Antiviral synergic effects of DN200434 with virus-targeting antiviral drugs *in vivo*.

Supplementary Files

This is a list of supplementary files associated with this preprint. Click to download.

- SupplementaryMaterialsandMethods.docx